Optimal UAV Positioning for Terrestrial-Aerial Communication in Presence of Fading

Mohammad Mahdi Azari*, Fernando Rosas†, Kwang-Cheng Chen†, and Sofie Pollin*
* Departement of Electrical Engineering, KU Leuven, Belgium
† Graduate Institute of Communication Engineering, National Taiwan University, Taipei, Taiwan
Email: mahdi.azari@esat.kuleuven.be

***Abstract*—Aerial communication platforms have been recently recognized as an effective solution to provide wireless access to terrestrial users, which promise to increase reliability and throughput thanks to their superior coverage capabilities. In this paper, we explore the impact of the height of an Unmanned Aerial Vehicle (UAV) on the area over which it can provide wireless service. We investigate the problem by characterizing the coverage area for a target outage probability, showing that for the case of Rician fading there exist a unique optimum height that maximizes the coverage area. The optimum UAV height guarantees a beneficial trade-off between path loss and fading, which vary as function of distance and the elevation angle with respect to the ground terminals. Moreover, a closed-form approximated solution is provided, which is valid for any functional dependency between the elevation angle and the Rician factor.**

***Index Terms*—Terrestrial–aerial communication, unmanned aerial vehicle (UAV), outage probability, Rician fading.**

I. Introduction

Aerial communication platforms have been acknowledged in recent years as an interesting alternative to provide wireless services for terrestrial users. Facebook Aquila Drone [1] and Google Loon [2] are two well-known projects that exploit aerial platforms to fill coverage gaps and provide internet access for users in remote locations. The ABSOLUTE project [3] is another important initiative that uses aerial platforms to improve public safety and achieve capacity enhancement.

The quick deployment of Unmanned Aerial Vehicles (UAVs) as aerial platforms, independent of terrestrial infrastructures, makes UAVs effectively applicable for many operations [4]–[6]. Recent reports show promising opportunities in integrating UAVs to heterogeneous networks, working either as base stations or relays [7]–[9]. In [7] the use of UAV for public safety communication has been studied where the legacy terrestrial infrastructure is damaged. Through simulations the authors showed that the throughput coverage can be improved by optimizing the location of the UAV. In [8] the airborne relays are utilized to assist the existing cellular networks by providing emergency coverage.

An important issue in the design of a terrestrial-aerial network is the effect that the UAV height has on the coverage performance, link reliability and service availability. In effect, interest on this issue has been reported in recent literature [10]–[12]. The optimal placement of the UAV was explored in [10] based on simulations, without providing a theoretical framework that could lead to a generalization of the results. The relationship between the UAV height and coverage area was analyzed in [11], [12], where the impact of altitude on the required transmit power was addressed as well in [12]. However, these works studied a deterministic coverage ignoring the effects of multipath and random fading, which are an essential feature of the wireless channel. To the best of our knowledge, there is no analytical study on the relationship between UAV height and coverage area that considers more realistic assumptions on the wireless link statistics.

In order to address this problem, a suitable model for the terrestrial-aerial communication channel is required. The Rician model is an adequate choice, as it can effectively reflect the combination of LoS and scattering that exists in the links between the UAV and ground nodes [13]–[15]. Interestingly, experimental evidence suggest that the Rician factor is affected by the link's elevation angle, as a higher UAV is more likely to experience LoS [16]–[19]. These results trigger the question whether it is possible to determine an optimal height for a UAV with respect to the resulting ground-to-air communication link, trading-off path loss due to the higher altitude with a reduced influence of multipath scattering.

In this paper, we consider a terrestrial-aerial communication network where a UAV provides wireless access to a number of ground nodes. By studying the outage probability of the network, we show that there exist an optimum height for the UAV which maximizes the coverage area. Moreover, we derive approximate closed-form expressions for the maximum coverage radius and optimal height of the UAV for the case of Rician fading. These expressions provide insights on the relationship between the maximum coverage area and signal to noise ratio (SNR) or transmission power requirements.

The rest of the paper is organized as follows. First, Section II presents the system model and Section III defines the problem statement. Then, the optimal UAV positioning and the maximum coverage area are investigated in Section IV. Section V presents numerical simulations that confirm and illustrate our results. Finally, our main conclusions are summarized in Section VI.

978-1-5090-1328-9/16/$31.00 ©2016 IEEE

II. System Model

We focus on a terrestrial-aerial communication network, where a UAV provides wireless connectivity to the nodes on the ground as shown in Figure 1. The UAV is located at an altitude of h meters, and the elevation angle with respect to a terrestrial node T is denoted as $\theta = \tan^{-1}(h/r_{\mathrm{T}})$, where r_{T} is the distance of the terrestrial node from the projection of the UAV onto the ground O.

A. Modeling the Channel

Let us consider the uplink communication channel from the node T to the UAV, which suffers from both random small-scale fading and deterministic large-scale path loss. The instantaneous SNR between the node T and the UAV can be expressed as

$$\Gamma_{\mathrm{T}} = \frac{AP_{\mathrm{T}}}{N_0 {\ell_{\mathrm{T}}}^{\alpha}}\ \Omega_{\mathrm{T}}, \tag{1}$$

where ℓ_{T} denotes the distance between T and the UAV, α is the path loss exponent, P_{T} is the radiated power at the transmitter, N_0 is the noise power, A is a constant that accounts the effects of system parameters such as antenna gain and operating frequency, and $\Omega_{\mathrm{T}} \in [0, \infty)$ is a random variable that corresponds to the effects of the small-scale fading such that $\overline{\Omega}_{\mathrm{T}} = 1$.

For modeling terrestrial-aerial communication links, which are usually composed by a combination of LoS and scattered signals, the Rician fading model is commonly used in the literature [13]–[15]. In this model, the distribution of Ω_{T} follows a non-central chi-square probability distribution function (PDF) given by [20]

$$f_{\Omega_{\mathrm{T}}}(\omega) = \frac{(K+1)e^{-K}}{\overline{\Omega}_{\mathrm{T}}}\ e^{\frac{-(K+1)\omega}{\overline{\Omega}_{\mathrm{T}}}}\ I_0\left(2\sqrt{\frac{K(K+1)\omega}{\overline{\Omega}_{\mathrm{T}}}}\right), \tag{2}$$

where $\omega \geq 0$, $I_0(\cdot)$ is the zero-order modified Bessel function of the first kind, and K is the Rician factor that corresponds to the ratio between the power of the LoS component and the power of the multipath components. It can be shown that for $K = 0$ the Rician model reduces to a Rayleigh fading distribution, whereas for $K \to \infty$ it converges to an AWGN channel. Hence, in general a small value of K represents a predominance of the multipath component while a large K corresponds to a strong LoS between transmitter and receiver.

B. Modeling the Rician Factor

Different terrestrial nodes might experience a different Rician factor while communicating with the same UAV, as the predominance of the LoS can vary across different locations. In [18], [19] is shown that the elevation angle θ plays a dominant role among the factors that influence the Rician factor. The reason for this is the fact that the terrestrial-aerial link is most likely to have a strong LoS as the elevation angle increases. From the measurements presented in these works, it can also be seen that other parameters that affect K are the carrier frequency and the antenna technology.

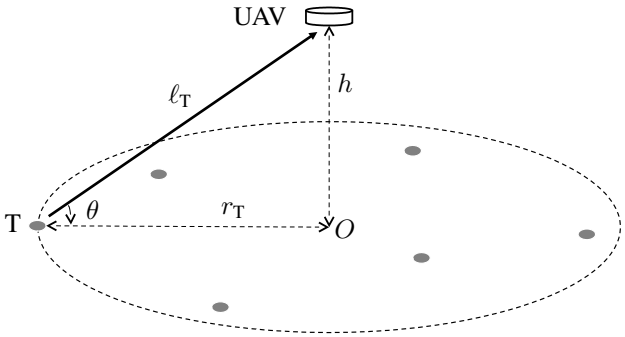

Fig. 1. A typical terrestrial-aerial communication system with a number of ground nodes and a UAV. A terrestrial node T, and the UAV share a communication link with elevation angle of θ.

Our approach in this paper is to consider a general relationship between K and θ characterized by the function $K = \Psi(\theta)$ for $\theta \in [0, \pi/2]$. Accordingly, and in consistency with the results presented in [18], [19], it is assumed that the dependency of K on different values of h and r_{T} is mainly determined by their ratio.

The main results presented in this paper do not require any specific functional form for the dependency between K and θ, but only that $\Psi(\cdot)$ is a differentiable and increasing function. However, for purposes of illustration, in Section V-A we adopt a concrete dependency for $\Psi(\theta)$ in order to provide numerical results.

III. Problem Formulation

In this section we formulate the problem of finding the optimal UAV height that maximizes the area to which it can provide wireless connectivity reliably. To this end, first the coverage area is defined based on the notion of outage probability.

For a given node T, the outage probability $\mathcal{P}_{out}$ of the terrestrial-aerial communication link is defined as

$$\mathcal{P}_{out} \triangleq \mathbb{P}(\Gamma_{\mathrm{T}} \leq \xi), \tag{3}$$

where $\mathbb{P}(\cdot)$ denotes the probability and ξ is an SNR threshold. Using (1) and (2) a direct computation shows that $\mathcal{P}_{out}$ in (3) can be rewritten as

$$\mathcal{P}_{out}(h, r_{\mathrm{T}}) = \mathbb{P}\left(\frac{AP_{\mathrm{T}}}{N_0 {\ell_{\mathrm{T}}}^{\alpha}}\ \Omega_{\mathrm{T}} \leq \xi\right) \tag{4a}$$

$$= 1 - Q\left(\sqrt{2\Psi(\theta)}, \sqrt{2\xi\ [1 + \Psi(\theta)]\ {\ell_{\mathrm{T}}}^{\alpha}/\beta_{\mathrm{T}}}\right), \tag{4b}$$

where $Q(\cdot, \cdot)$ is the first-order Marcum Q–function [21] and $\beta_{\mathrm{T}} = AP_{\mathrm{T}}/N_0$ is a shorthand notation (recall that $\theta = \tan^{-1}(h/r_{\mathrm{T}})$ and $\ell_{\mathrm{T}} = \sqrt{r_{\mathrm{T}}^2 + h^2}$ are functions of r_{T} and h).

A terrestrial-aerial communication link is considered reliable if its outage probability is sufficiently small, i.e. if

$$\mathcal{P}_{out}(h, r_{\mathrm{T}}) \leq \epsilon, \tag{5}$$

where ϵ is a constant defined by the desired quality of service. The *coverage area* of a UAV that stays at height h, denoted as $\mathcal{C}_h$, is composed by all the locations that can host reliable links. Equivalently, $\mathcal{C}_h$ is the geographical region of points whose r_{T} satisfies (5).

As nodes that are closer to the UAV experience a stronger link, in general the coverage area is a disc centered at O. The radius of the coverage area for a given UAV height h, denoted as ρ_h, can be found by solving the implicit equation over ρ_h:

$$\mathcal{P}_{out}(h, \rho_h) = \epsilon, \tag{6}$$

which can be rewritten using (4b) as

$$Q\left(\sqrt{2\Psi(\theta)}, \sqrt{2\xi\ [1+\Psi(\theta)]\ {\ell_{\mathrm{T}}}^{\alpha}/\beta_{\mathrm{T}}}\right) = 1-\epsilon. \tag{7}$$

The set of all pairs (h, ρ_h) that satisfy (7) form the *configuration space* of the system, denoted as $\mathcal{S}$.

Our interest is to find the optimal altitude $\hat{h}$ at which the UAV should be located in order to maximize the coverage area. In other words, by denoting the maximum coverage radius as $\hat{\rho}_h$, we seek the pair $(\hat{h}, \hat{\rho}_h)$ that satisfies

$$\hat{\rho}_h = \max_{h\in[0,\infty)} \rho_h\ , \quad \hat{h} = \{h \mid (h, \hat{\rho}_h) \in \mathcal{S}\}\,. \tag{8}$$

IV. Maximum Coverage Area

For solving (7), our approach is based on using an approximation to the inverse Marcum Q–function. Most of the existent approaches for computing the inverse Marcum Q–function are iterative [21], [22], and hence they cannot be written in closed-form. In contrast, we propose a closed-form approximation that is accurate in the range of interest for our problem. Using this approximation, Theorem 1 presents a formula for computing the maximum coverage radius and optimum UAV height as defined in Section III.

To present our approximation of the inverse Marcum Q–function, assume that for a given value of y and ϵ, $z = Q^{-1}(y, 1-\epsilon)$ provides the value of z that satisfies the solution of $Q(y,z) = 1-\epsilon$. We approximate $Q^{-1}(y, 1-\epsilon)$ in the following lemma.

Lemma 1. *If $\epsilon < 0.1$ then the value of $z = Q^{-1}(y, 1-\epsilon)$ can be approximated by*

$$z \simeq y - c_\epsilon;\ \ c_\epsilon = -0.015\,[\ln(\epsilon)]^2 - 0.529\,\ln(\epsilon) + 0.122. \tag{9}$$

Proof. The proof is given in Appendix A. □

Using (9), the configuration space $\mathcal{S}$ can be characterized as follows.

Lemma 2. *The configuration space $\mathcal{S}$ is a one-dimensional curve in $r_T - h$ plane, which can be parameterized by*

$$h(y) = \Lambda(y)\cdot\sin\theta(y)\ , \quad \rho_h(y) = \Lambda(y)\cdot\cos\theta(y)\ , \tag{10a}$$

where

$$\Lambda(y) = \left(\frac{\beta_T\ [y-c_\epsilon]^2}{\xi\ [2+y^2]}\right)^{\frac{1}{\alpha}}\ , \quad \theta(y) = \Psi^{-1}\left(\frac{y^2}{2}\right) \tag{10b}$$

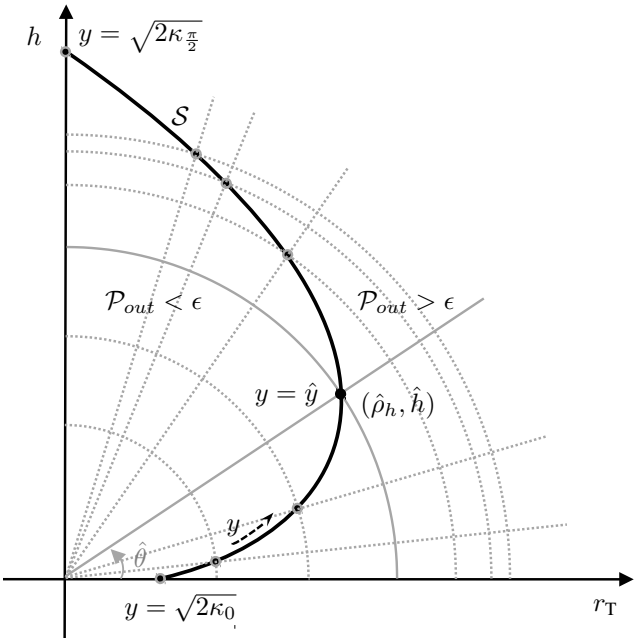

Fig. 2. A geometric illustration of the configuration space $\mathcal{S}$. The shape of $\mathcal{S}$ shows that for low altitudes the reduction of the multipath effect provided by an increase of height is beneficial. However, for high altitudes the path loss dominates and hence increasing the height is harmful. A unique optimal height lays between these two regimes.

and $y \in [\sqrt{2\kappa_0}, \sqrt{2\kappa_{\frac{\pi}{2}}}]$ where $\kappa_0 = \Psi(0)$ and $\kappa_{\frac{\pi}{2}} = \Psi(\pi/2)$ are the minimum and maximum values of $K = \Psi(\theta)$, respectively.

Proof. Using $y = \sqrt{2\Psi(\theta)}$ as an auxiliary variable, θ can be written as

$$\theta(y) = \Psi^{-1}\left(\frac{y^2}{2}\right) \tag{11}$$

where $\Psi^{-1}(\cdot)$ indicates the inverse function of $\Psi(\cdot)$. From Lemma 1, (7) is equivalent to

$$\sqrt{\frac{2[1+\Psi(\theta)]\ \xi{\ell_{\mathrm{T}}}^{\alpha}}{\beta_{\mathrm{T}}}} = y - c_\epsilon. \tag{12}$$

By replacing $\Psi(\theta) = y^2/2$ into (12) and rewriting it one obtains

$$\ell_{\mathrm{T}} = \left(\frac{\beta_T\ [y-c_\epsilon]^2}{\xi\ [2+y^2]}\right)^{\frac{1}{\alpha}} \triangleq \Lambda(y). \tag{13}$$

Knowing that $h = \ell_{\mathrm{T}}\sin\theta$ and $\rho_h = \ell_{\mathrm{T}}\cos\theta$, and using the equations (11) and (13), the desired results are attained. □

Above, $\Lambda(y)$ and $\theta(y)$ correspond to the radius and angle of the curve $\mathcal{S}$ given in polar coordinates (see Figure 2). For $y = \sqrt{2\kappa_0}$ one sees that $\theta(y) = 0$ resulting in $h(y) = 0$ and $\rho_h(y) = \Lambda(\sqrt{2\kappa_0})$, whereas for $y = \sqrt{2\kappa_{\frac{\pi}{2}}}$, $\theta(y) = \pi/2$ resulting in $h(y) = \Lambda(\sqrt{2\kappa_{\frac{\pi}{2}}})$ and $\rho_h(y) = 0$.

The value of y that yields the optimal height and the maximum coverage radius is characterized in the next theorem.

Theorem 1. *The value of $y = \hat{y}$ at which $h(\hat{y}) = \hat{h}$ and $\rho_h(\hat{y}) = \hat{\rho}_h$ can be found from*

$$\hat{y}^2 = 2\Psi\left\{\tan^{-1}\left(\frac{2\,(2+c_\epsilon\hat{y})}{\alpha\hat{y}\;(2+\hat{y}^2)\,(\hat{y}-c_\epsilon)}\;\Psi'\left[\Psi^{-1}\left(\frac{\hat{y}^2}{2}\right)\right]\right)\right\}, \tag{14}$$

where $\Psi'(\cdot)$ indicates the derivative function of $\Psi(\cdot)$.

Proof. The proof can be found in Appendix B. □

Corollary 1. *The elevation angle that corresponds to the boundary of the maximum coverage area, $\hat{\theta} = \tan^{-1}(\hat{h}/\hat{\rho}_h)$, can be found by solving*

$$\tan\hat{\theta} = \frac{\left(2+c_\epsilon\sqrt{2\Psi(\hat{\theta})}\right)}{\alpha\sqrt{2\Psi(\hat{\theta})}(1+\Psi(\hat{\theta}))\left(\sqrt{2\Psi(\hat{\theta})}-c_\epsilon\right)}\;\Psi'(\hat{\theta}). \tag{15}$$

Proof. This equation is obtained by rewriting (37) in terms of $\theta = \hat{\theta}$ which relates to $y = \hat{y}$ using (11). □

The results in (14) and (15) show that $\hat{y}$ and $\hat{\theta}$ are determined by ϵ and the propagation parameters, i.e. α and $\Psi(\cdot)$, being independent of the transmit power and SNR threshold. Therefore, from (10) one sees that the maximum coverage radius and optimum height are proportional to $\sqrt[\alpha]{\beta_{\mathrm{T}}}$ and $\sqrt[-\alpha]{\xi}$. In the following, (15) is instantiated for the case of free-space transmissions where $\alpha = 2$.

Corollary 2. *If $\alpha = 2$, the approximate $\hat{y}$ and $\hat{\theta}$ can be obtained from the equations*

$$\tan\Psi^{-1}\left(\frac{\hat{y}^2}{2}\right) = \frac{c_\epsilon}{\hat{y}^2\,(\hat{y}-c_\epsilon)}\;\Psi'\left[\Psi^{-1}\left(\frac{\hat{y}^2}{2}\right)\right] \tag{16a}$$

and

$$\tan\hat{\theta} = \frac{c_\epsilon}{2\Psi(\hat{\theta})\left(\sqrt{2\Psi(\hat{\theta})}-c_\epsilon\right)}\;\Psi'(\hat{\theta}). \tag{16b}$$

Proof. With $\alpha = 2$ and assuming $y \gg \sqrt{2}$, $\Lambda(y)$ in (10b) can be simplified as

$$\Lambda(y) \simeq \frac{y-c_\epsilon}{y}\sqrt{\frac{\beta_T}{\xi}}. \tag{17}$$

Hence, by taking the derivative of $\Lambda(y)$ and using (33) and the first equation in (35) one can write

$$\tan\theta = \frac{c_\epsilon/y^2}{([y-c_\epsilon]/y)\,(y/\Psi'(\theta))} = \frac{c_\epsilon}{y^2[y-c_\epsilon]}\Psi'(\theta). \tag{18}$$

By using (11) in the above equation the desired results for $y = \hat{y}$ and $\theta = \hat{\theta}$ are obtained. □

V. Case Study: Exponential Dependency Between K and θ

This section illustrates our results by instantiating the expressions for an exponential dependency between the Rician factor and the elevation angle. In the sequel, a model for K is presented in Section V-A and then numerical evaluations are presented in Section V-B.

A. Model for K

Let us assume that the dependency of K and θ is given by

$$K = \Psi(\theta) = ae^{b\theta}, \tag{19}$$

where a and b are constants depending on the environment and on the system parameters. Such dependency is supported by the empirical data presented in [18]. The constants a and b can be determined as

$$a = \kappa_0, \quad b = \frac{2}{\pi}\ln\left(\frac{\kappa_{\frac{\pi}{2}}}{\kappa_0}\right), \tag{20}$$

where κ_0 and $\kappa_{\frac{\pi}{2}}$ are as defined in Lemma 2 and could be determined from measurements in a concrete scenario.

In the sequel, Corollary 2 is specialized with the proposed exponential model for K.

Corollary 3. *Considering* (19)*, the optimal values $\hat{y}$ and $\hat{\theta}$ can be found for $\alpha = 2$ by solving*

$$\tan\left(\frac{2\ln(\hat{y})-\ln(2a)}{b}\right) = \frac{bc_\epsilon}{2(\hat{y}-c_\epsilon)} \tag{21a}$$

and

$$\tan\hat{\theta} = \frac{bc_\epsilon}{2(\sqrt{2ae^{b\hat{\theta}}}-c_\epsilon)}. \tag{21b}$$

Proof. From (19) one finds that

$$\Psi'(\theta) = abe^{b\theta} = b\;\Psi(\theta) \tag{22a}$$

and

$$\Psi^{-1}\left(\frac{y^2}{2}\right) = \frac{2\ln(y)-\ln(2a)}{b}. \tag{22b}$$

From (16), (19) and (22) the desired results are reached. □

Note that the left-hand side expression of (21a) is a continuous strictly increasing function of $\hat{y}$ while the right-hand side term is continuous strictly decreasing. Moreover, the former function varies from 0 to $+\infty$ while the latter reaches $+\infty$ at one point and then as $\hat{y} \to \sqrt{2\kappa_{\pi/2}}$, decreases up to a very small positive number. Thus, these two functions cross each other at exactly one point, which is the unique solution to the equation.

B. Numerical Results

We performed numerical evaluations for illustrating the results presented in the previous sections. In this analysis, it is assumed that $\beta_T = 70$ dB, $\xi = 5$ dB, $\alpha = 2$, $\epsilon = 0.001$, and $(\kappa_0, \kappa_{\frac{\pi}{2}}) = (3, 30)$ dB unless otherwise is mentioned.

Results show that, the outage probability increases with r_{T}, however it can be minimized by optimizing the UAV altitude for a given r_{T} (see Figure 3). Indeed, increasing altitude h results in a longer link length that increases the path loss. However, increasing h also leads to a larger elevation angle resulting in a larger K, which means that the negative effect of multipath scattering is reduced. For low altitudes the effect of reducing the multipath effect is highly beneficial such that the outage probability decreases steeply with the height, while for high altitudes the increase in the path loss becomes dominant resulting in increasing

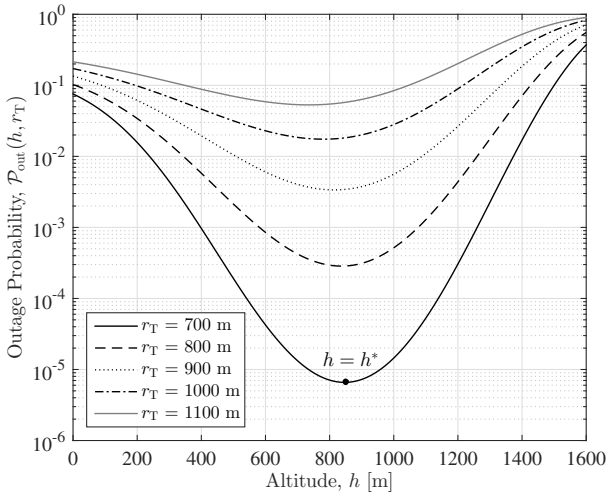

Fig. 3. By varying the UAV height, the outage probability can be minimized for each terrestrial node location. Note that in this simulation the Rician factor increases exponentially with the elevation angle as given in (19).

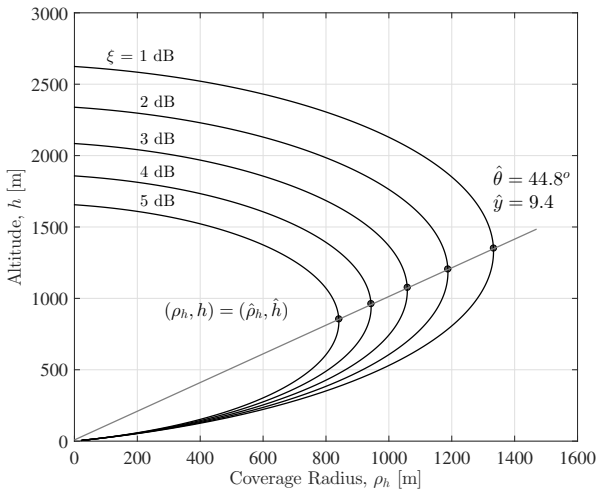

Fig. 5. The locus of the configuration space for $\epsilon = 0.001$. The maximum coverage radius and the optimum height proportionally decrease as the SNR threshold increases.

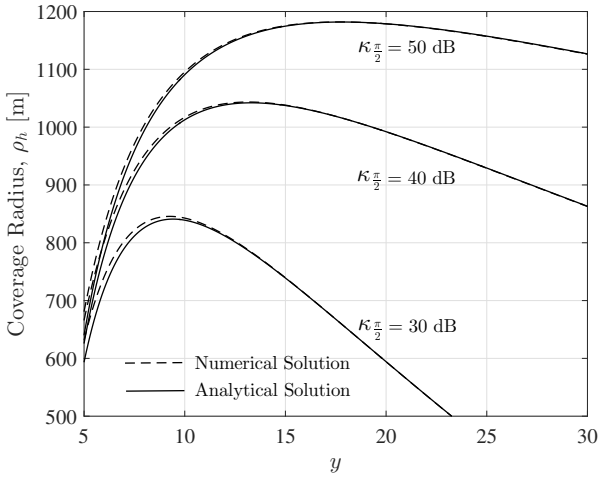

Fig. 4. Dependency of the coverage radius and the free parameter y for an exact numerical solution and for the approximated closed-form expression as epressed in (10). Results show the accuracy of our solution.

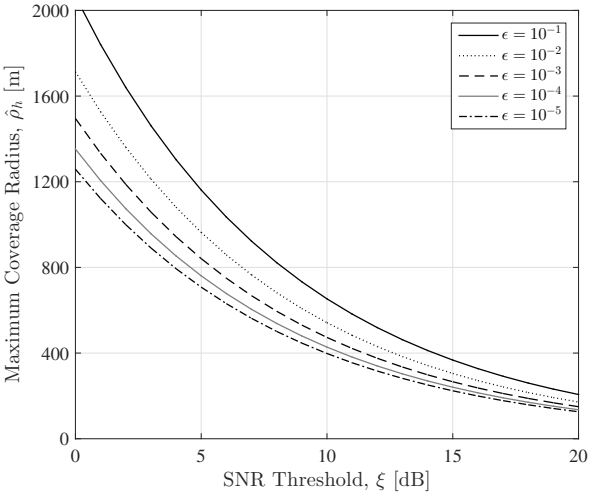

Fig. 6. The maximum coverage radius $\hat{\rho}_h$ decreases for higher requirements of received SNR. The curves show that the radius is proportinal to $\sqrt{\xi^{-1}}$.

outage probability. The point at which these two effects are balanced is the optimal height for the given r_{T}, denoted as h^* in the figure.

In Figure 4, the curves representing the numerical solution are obtained using the numerical method for computing the inverse Marcum Q–function whereas the analytical values are calculated with the proposed approximate closed-form expression for the inverse Marcum Q–funtion from Lemma 2. The results in Figure 4 confirm that the closed-form solution matches the numerical solution closely. The curves peak at $(y, \rho_h) = (\hat{y}, \hat{\rho}_h)$ where the analytical maximum coverage radius $\hat{\rho}_h$ differs only 0.6%, 0.1%, and 0% at $\kappa_{\pi/2} = 30$, 40, 50 dB respectively with the ones determined numerically. Moreover, from the figure it can be seen that for larger $\kappa_{\frac{\pi}{2}}$ leading to larger K, the maximum coverage radius increases.

The locus of the configuration space is depicted in Figure 5. As expected, for each altitude the coverage area diminishes with the SNR threshold ξ, however the reduction is larger for higher altitudes. Noticing the locations of $(\rho_h, h) = (\hat{\rho}_h, \hat{h})$, which are marked in the figure, the ratios of $\hat{h}/\hat{\rho}_h = \tan(\hat{\theta})$ for all examined ξs are constant and equal to 0.99 confirming that $\hat{\theta}$ and $\hat{h}/\hat{\rho}_h$ are independent from ξ as discussed in the previous section. However, the value of $\hat{\rho}_h$ is a decreasing function of ξ as depicted in Figure 6. Indeed, increasing ξ deteriorates the outage probability which results in a smaller coverage area for the same target outage constraint ϵ. This figure also confirms

that $\hat{\rho}_h \propto \sqrt{\xi^{-1}}$ which is discussed in the previous section. Due to the fact that the ratio of $\hat{h}/\hat{\rho}_h$ is fixed, $\hat{h}$ should have the same relation with ξ as $\hat{\rho}_h$. Furthermore, the impact of ϵ on the maximum coverage radius is shown in this figure where the increase of ϵ leads to a larger coverage area. The increase of $\hat{\rho}_h$ from $\epsilon = 10^{-4}$ to $\epsilon = 10^{-3}$ is 10% at $\xi = 5$ dB whereas from $\epsilon = 10^{-2}$ to $\epsilon = 10^{-1}$ the coverage radius increases with 20% meaning that in a larger ϵ the maximum coverage radius is more susceptible to ϵ.

VI. Conclusion

We analyzed a ground-to-air communication network composed of a UAV that provides wireless access to a number of ground nodes. We considered that the ground-to-air links suffer from path loss and scattering, and studied the optimal trade-off between them. By assuming a Rician fading model with K depending on the elevation angle, we showed that there exists a unique optimum height at which the UAV should be located in order to maximize the coverage area. Explicit formulas for the optimal height and maximum coverage radius were provided. Finally, our results were confirmed for the case of an exponential dependency between the Rician factor and the elevation angle.

Appendix A
Proof of Lemma 1

From [21] one can find that

$$\frac{\partial}{\partial y}\, Q(y,z) = z\; e^{-\frac{y^2+z^2}{2}}\; I_1(yz) > 0 \tag{23a}$$

and

$$\frac{\partial}{\partial z}\, Q(y,z) = -z\; e^{-\frac{y^2+z^2}{2}}\; I_0(yz) < 0, \tag{23b}$$

where $\mathrm{I}_1(\cdot)$ is the first order modified Bessel function and, similar to $\mathrm{I}_0(\cdot)$, it gives positive real numbers except at 0. Therefore, $Q(y,z)$ is respectively a strictly increasing and strictly decreasing function of y and z. Since $Q(y,z)$ is strictly decreasing function of z, $Q^{-1}(y,1-\epsilon) = z$ should be strictly increasing function of $\epsilon = 1 - Q(y,z)$ as well. Now, suppose that $z_1 = Q^{-1}(y_1, 1-\epsilon)$ and $z_2 = Q^{-1}(y_2, 1-\epsilon)$, or equivalently $Q(y_1, z_1) = 1-\epsilon$ and $Q(y_2, z_2) = 1-\epsilon$ such that $y_1 > y_2$. As $Q(y,z)$ is strictly increasing function of y one can write

$$Q(y_2, z_2) = 1 - \epsilon = Q(y_1, z_1) > Q(y_2, z_1). \tag{24}$$

Thus $Q(y_2, z_2) > Q(y_2, z_1)$ which implies $z_1 > z_2$ since $Q(y,z)$ is strictly decreasing function of z. To sum up, from $y_1 > y_2$ we conclude that $z_1 > z_2$ which means that $Q^{-1}(y, 1-\epsilon)$ is strictly increasing function of y.

We take the numerical solution of the equation for $\epsilon = \epsilon_{\min},\ \epsilon_{\max}$ using the iterative algorithm presented in [21] where $\epsilon_{\min} \to 0$ and $\epsilon_{\max} = 0.1$. The linear curves $z = y - 1.239$ and $z = y - 5.045$ are the best fitting curves to the numerical solutions corresponding to $\epsilon = \epsilon_{\max}$ and $\epsilon = \epsilon_{\min}$ respectively, which are illustrated in Figure 7. Thus one can write

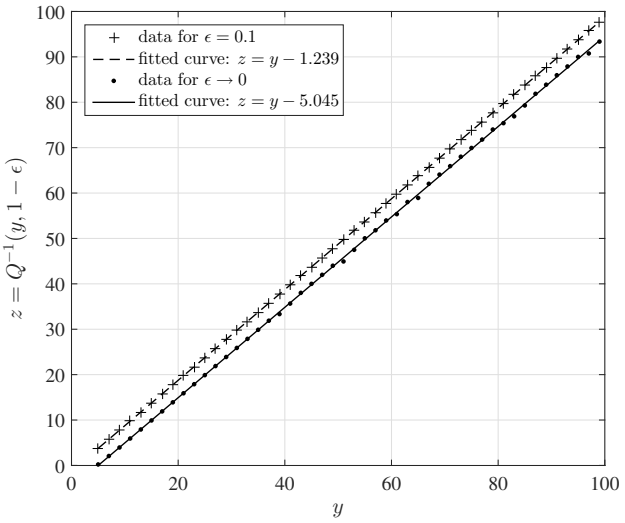

Fig. 7. The fitted curves to the values of $z = Q^{-1}(y, 1-\epsilon)$ obtained by the numerical method for $\epsilon = 10^{-1}$ and $\epsilon = 10^{-5}$, which are $z = y - 1.239$ and $z = y - 5.045$ respecively.

$$\begin{aligned} Q^{-1}(y, 1-\epsilon_{\max}) &= y - 1.239 + \delta_1(y, 1-\epsilon_{\max}), \\ Q^{-1}(y, 1-\epsilon_{\min}) &= y - 5.045 + \delta_2(y, 1-\epsilon_{\min}), \end{aligned} \tag{25}$$

where $\delta_1(y, 1-\epsilon_{\max})$ and $\delta_2(y, 1-\epsilon_{\min})$ are the negligible functions of y and $\epsilon_{\max}$, and y and $\epsilon_{\min}$ respectively. Now for $\epsilon_{\min} < \epsilon < \epsilon_{\max}$ we have

$$Q^{-1}(y, 1-\epsilon_{\min}) < Q^{-1}(y, 1-\epsilon) < Q^{-1}(y, 1-\epsilon_{\max}) \tag{26}$$

or equivalently for $z = Q^{-1}(y, 1-\epsilon)$ we obtain

$$y - 5.045 + \delta_2(y, 1-\epsilon_{\min}) < z < y - 1.239 + \delta_1(y, 1-\epsilon_{\max}). \tag{27}$$

Due to the tight upper and lower bounds for z specifically for large values of y, the value of z can be expressed as

$$z = y - c_\epsilon + \delta(y, 1-\epsilon) \tag{28}$$

where c_ϵ should be a decreasing function of ϵ and $\delta(y, 1-\epsilon)$ is a negligible function of y and ϵ. We interpolate the function c_ϵ using the samples $\epsilon = 10^{-1}, 10^{-2}, 10^{-3}, 10^{-4}, 10^{-5}$ where $c_\epsilon = 1.239, 2.281, 3.042, 3.667, 4.21$ are obtained respectively. The quadratic polynomial function of $\ln(\epsilon)$ which is $c_\epsilon = -0.015\ [\ln(\epsilon)]^2 - 0.529\ \ln(\epsilon) + 0.122$ is proposed by the sample values of c_ϵ. Replacing this function into (28) we finally have

$$z \simeq y - \big(-0.015\ [\ln(\epsilon)]^2 - 0.529\ \ln(\epsilon) + 0.122\big) \tag{29}$$

Appendix B
Proof of Theorem 1

In order to find $\hat{\rho}_h$, the value of y in Lemma 2 that maximizes $\rho_h(y)$ is to be found. Therefore, for $y = \hat{y}$ we should have

$$\frac{\partial}{\partial y}\rho_h(y) = 0. \tag{30}$$

Using (10a), the above equation can be written as

$$\frac{\partial \Lambda(y)}{\partial y}\ \cos\theta(y) + \Lambda(y)\ \frac{\partial \cos\theta(y)}{\partial y} = 0 \tag{31}$$

or equivalently

$$\frac{\partial \Lambda(y)}{\partial y}\ \cos\theta(y) - \Lambda(y)\ \sin\theta(y)\ \frac{\partial \theta(y)}{\partial y} = 0 \tag{32}$$

Thus,

$$\tan\theta = \frac{\frac{\partial \Lambda(y)}{\partial y}}{\Lambda(y)\ \frac{\partial \theta(y)}{\partial y}}. \tag{33}$$

Since $y = \sqrt{2\Psi(\theta)}$ or equivalently $\Psi(\theta) = y^2/2$, by taking derivative with respect to y one obtains

$$\frac{\partial \theta(y)}{\partial y}\Psi'(\theta) = y \tag{34}$$

or equivalently

$$\frac{\partial \theta(y)}{\partial y} = \frac{y}{\Psi'(\theta)} = \frac{y}{\Psi'\left(\Psi^{-1}\left(\frac{y^2}{2}\right)\right)}, \tag{35}$$

where the last equation is obtained from (10b). Using (10b) and (35) in (33) yields

$$\tan\Psi^{-1}\left(\frac{y^2}{2}\right) = \frac{\Psi'\left(\Psi^{-1}\left(\frac{y^2}{2}\right)\right)}{y\ \sqrt{\Lambda_1(y)}}\ \frac{\partial\sqrt{\Lambda_1(y)}}{\partial y}. \tag{36}$$

By replacing $\Lambda(y)$ from (10b) into (36) and simplifying it, we obtain

$$\tan\Psi^{-1}\left(\frac{y^2}{2}\right) = \frac{2\,(2+yc_\epsilon)}{\alpha y(2+y^2)\,(y-c_\epsilon)}\ \Psi'\left[\Psi^{-1}\left(\frac{y^2}{2}\right)\right]. \tag{37}$$

The solution of (37), i.e. $y = \hat{y}$, equivalently satisfies

$$\hat{y}^2 = 2\Psi\left\{\tan^{-1}\left(\frac{2\,(2+\hat{y}c_\epsilon)}{\alpha\hat{y}\ (2+\hat{y}^2)\,(\hat{y}-c_\epsilon)}\ \Psi'\left[\Psi^{-1}\left(\frac{\hat{y}^2}{2}\right)\right]\right)\right\}.$$

REFERENCES

[1] Facebook, *Connecting the World from the Sky*. Facebook, Technical Report, 2014.

[2] S. Katikala, "Google project loon," *InSight: Rivier Academic Journal*, vol. 10, no. 2, 2014.

[3] *ABSOLUTE (Aerial Base Stations with Opportunistic Links for Unexpected and Temporary Events)*. http://www.absolute-project.eu.

[4] C. Wu, X. Cao, R. Lin, and F. Wang, "Registration-based moving vehicle detection for low-altitude urban traffic surveillance," in *Intelligent Control and Automation (WCICA), 2010 8th World Congress on*. IEEE, 2010, pp. 373–378.

[5] L. Reynaud and T. Rasheed, "Deployable aerial communication networks: challenges for futuristic applications," in *Proceedings of the 9th ACM symposium on Performance evaluation of wireless ad hoc, sensor, and ubiquitous networks*. ACM, 2012, pp. 9–16.

[6] A. Qiantori, A. B. Sutiono, H. Hariyanto, H. Suwa, and T. Ohta, "An emergency medical communications system by low altitude platform at the early stages of a natural disaster in indonesia," *Journal of medical systems*, vol. 36, no. 1, pp. 41–52, 2012.

[7] A. Merwaday and I. Guvenc, "Uav assisted heterogeneous networks for public safety communications," in *Wireless Communications and Networking Conference Workshops (WCNCW)*. IEEE, 2015, pp. 329–334.

[8] W. Guo, C. Devine, and S. Wang, "Performance analysis of micro unmanned airborne communication relays for cellular networks," in *Communication Systems, Networks & Digital Signal Processing (CSNDSP), 2014 9th International Symposium on*. IEEE, 2014, pp. 658–663.

[9] S. Rohde and C. Wietfeld, "Interference aware positioning of aerial relays for cell overload and outage compensation," in *Vehicular Technology Conference (VTC Fall)*. IEEE, 2012, pp. 1–5.

[10] J. Kosmerl and A. Vilhar, "Base stations placement optimization in wireless networks for emergency communications," in *Communications Workshops (ICC), 2014 IEEE International Conference on*. IEEE, 2014, pp. 200–205.

[11] A. Al-Hourani, S. Kandeepan, and S. Lardner, "Optimal lap altitude for maximum coverage," *Wireless Communications Letters, IEEE*, vol. 3, no. 6, pp. 569–572, 2014.

[12] M. Mozaffari, W. Saad, M. Bennis, and M. Debbah, "Drone small cells in the clouds: Design, deployment and performance analysis," *arXiv preprint arXiv:1509.01655*, 2015.

[13] S. Kandeepan, K. Gomez, L. Reynaud, and T. Rasheed, "Aerial-terrestrial communications: terrestrial cooperation and energy-efficient transmissions to aerial base stations," *Aerospace and Electronic Systems, IEEE Transactions on*, vol. 50, no. 4, pp. 2715–2735, 2014.

[14] S. Kandeepan, K. Gomez, T. Rasheed, and L. Reynaud, "Energy efficient cooperative strategies in hybrid aerial-terrestrial networks for emergencies," in *Personal Indoor and Mobile Radio Communications (PIMRC), 2011 IEEE 22nd International Symposium on*, 2011, pp. 294–299.

[15] D. W. Matolak, "Air-ground channels & models: Comprehensive review and considerations for unmanned aircraft systems," in *Aerospace Conference, 2012 IEEE*, 2012, pp. 1–17.

[16] E. Haas, "Aeronautical channel modeling," *Vehicular Technology, IEEE Transactions on*, vol. 51, no. 2, pp. 254–264, 2002.

[17] D. W. Matolak and R. Sun, "Unmanned aircraft systems: Air-ground channel characterization for future applications," *Vehicular Technology Magazine, IEEE*, vol. 10, no. 2, pp. 79–85, 2015.

[18] J. Hagenauer, F. Dolainsky, E. Lutz, W. Papke, and R. Schweikert, "The maritime satellite communication channel–channel model, performance of modulation and coding," *Selected Areas in Communications, IEEE Journal on*, vol. 5, no. 4, pp. 701–713, 1987.

[19] S. Shimamoto *et al.*, "Channel characterization and performance evaluation of mobile communication employing stratospheric platforms," *IEICE transactions on communications*, vol. 89, no. 3, pp. 937–944, 2006.

[20] M. K. Simon and M.-S. Alouini, *Digital communication over fading channels*. John Wiley & Sons, 2005, vol. 95.

[21] R. T. Short, "Computation of rice and noncentral chi-squared probabilities," 2012.

[22] A. Gil, J. Segura, and N. M. Temme, "The asymptotic and numerical inversion of the marcum q-function," *Studies in Applied Mathematics*, vol. 133, no. 2, pp. 257–278, 2014.